

(introducing strains), an oxid layer, or absorbed gases, increase the  $\kappa$  value of the surface material and lead to a reduced critical current. This is in accord with recent work of LeBlanc.<sup>29</sup>

*Note added in proof.* Recently, J. G. Park has presented calculations of Eq. (1) [Phys. Rev. Letters **16**, 1196 (1966)] which he claims are more accurate than ours<sup>7</sup> in several respects. He claims to have included the minimization of the free energy with respect to the vector potential in the calculation of Eq. (1); however, he appears to have made the same approximation that

<sup>29</sup> M. A. R. LeBlanc, Phys. Letters **21**, 266 (1966).

we did,<sup>7</sup> namely, he assumes that one can ignore the effect of the total current density  $J_o$  upon the order parameter of the sheath. Our values of  $\Delta/\xi$  and  $F^2(R)$  (see text) were taken from Ref. 6 in which the total current was taken to be zero.

#### ACKNOWLEDGMENTS

We would like to acknowledge the assistance of H. G. James in sample preparation and data reduction. We would also like to thank R. R. Hake, A. S. Joseph, and W. J. Tomasch for informative discussions.

## Proton and Chlorine Nuclear Magnetic Resonance in Antiferromagnetic $\text{MnCl}_2 \cdot 4\text{H}_2\text{O}$ †

R. D. SPENCE AND V. NAGARAJAN

*Department of Physics, Michigan State University, East Lansing, Michigan*

(Received 21 April 1966)

The magnetic structure of the antiferromagnetic phase of  $\text{MnCl}_2 \cdot 4\text{H}_2\text{O}$  has been examined using proton and chlorine NMR. By combining observations on the symmetry and number of proton internal magnetic fields with x-ray and neutron-diffraction data, one is led to three possible magnetic structures. However, only one of these ( $P2_1/a'$ ) predicts fields at the proton sites whose orientation and magnitude is in reasonable agreement with the experimentally observed fields. The chlorine resonance data corroborate the proton-resonance results and provide information on the transferred hyperfine interaction.

### I. INTRODUCTION

ALTHOUGH the antiferromagnetic phase of  $\text{MnCl}_2 \cdot 4\text{H}_2\text{O}$  has been the subject of a number of experimental investigations, very little appears to be known of the antiferromagnetic spin arrangement. The form of the  $H$ - $T$  phase diagram<sup>1</sup> and the temperature dependence of the magnetic susceptibility<sup>2</sup> indicate that  $\text{MnCl}_2 \cdot 4\text{H}_2\text{O}$  is probably a simple two-sublattice antiferromagnet with a rather small but quite anisotropic molecular field which results in a low Néel temperature (1.62°K)<sup>3,4</sup> and a sublattice magnetization along the  $c$  axis. The work reported here deals with an experimental study of the proton and chlorine nuclear resonance in the antiferromagnetic phase. The main objective is to obtain the spin arrangement which is inferred by combining the nuclear-resonance data with the crystal-structure data considered in the next section.

### II. CRYSTAL STRUCTURE

According to Zalkin, Forrester, and Templeton,<sup>5</sup> the structure of the modification of  $\text{MnCl}_2 \cdot 4\text{H}_2\text{O}$  which grows at room temperature is as shown in Fig. 1. In discussing the interrelation of the magnetic properties and the crystal structure, two different unit cells are useful. The first outlined by solid lines in Fig. 1 has dimensions  $a_1=11.186$  Å,  $b_1=9.513$  Å,  $c_1=6.186$  Å, and  $\beta_1=99.74^\circ$ . The space group is  $P2_1/n$  and there are four formula units in the cell. This cell is that used by Zalkin, Forrester, and Templeton and by Groth<sup>6</sup> in his morphological description of the crystal. The second unit is shown by dashed lines in Fig. 1. Its dimensions are  $a_2=11.830$  Å,  $b_2=9.513$  Å,  $c_2=6.186$  Å, and  $\beta_2=111.27^\circ$ . The space group is  $P2_1/a$  and there are again four molecules in the unit cell. The latter cell was used by Delain<sup>7</sup> in earlier x-ray work. It has the advantage that it locates the symmetry elements in conventional places in the unit cell and permits the use of conventional notation when discussing the *magnetic* space group of the crystal.

† This work supported by the U. S. Air Force Office of Scientific Research.

<sup>1</sup> H. M. Gijsman, N. J. Poullis, and J. Van Den Handel, *Physica* **25**, 954 (1959).

<sup>2</sup> M. A. Lasheen, J. Van Den Brock, and C. J. Gorter, *Physica* **24**, 1061 (1958).

<sup>3</sup> W. E. Henry, *Phys. Rev.* **91**, 431 (1953).

<sup>4</sup> S. A. Friedberg and J. D. Wasscher, *Physica* **19**, 1072 (1953).

<sup>5</sup> A. Zalkin, J. D. Forrester, and D. H. Templeton, *Inorg. Chem.* **3**, 529 (1964).

<sup>6</sup> P. Groth, *Chemische Kristallographie* (Wilhelm Englemann, Leipzig, 1908), Vol. I.

<sup>7</sup> C. Delain, *Compt. Rend.* **238**, 1245 (1954).

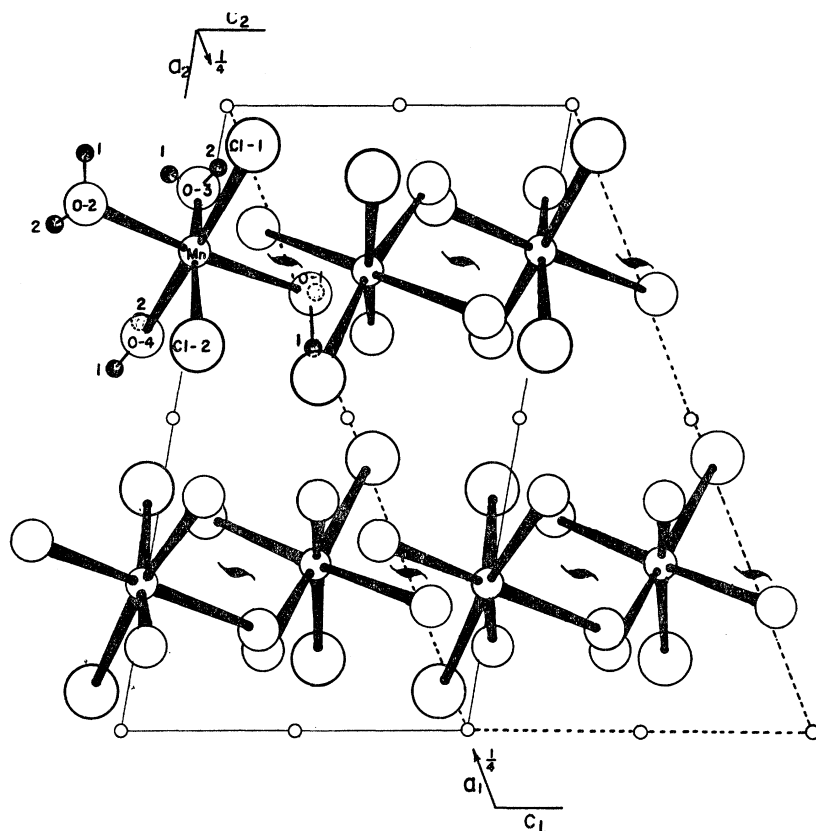


FIG. 1. The structure of  $\text{MnCl}_2 \cdot 4\text{H}_2\text{O}$ . The solid and dotted lines outline the alternate unit cells.

All atoms lie in general fourfold positions related by the screw axes, glide planes and inversion centers shown in the figure. Each manganese ion is the center of a distorted coordination octahedron consisting of four water oxygens and two chlorines. The most remarkable feature of the structure is the fact that the chlorines lie in adjacent positions on the octahedron rather than opposite to each other as in  $\text{FeCl}_2 \cdot 4\text{H}_2\text{O}$ ,<sup>8</sup>  $\text{NiCl}_2 \cdot 6\text{H}_2\text{O}$ <sup>9</sup> and  $\text{CoCl}_2 \cdot 6\text{H}_2\text{O}$ .<sup>10</sup> The Mn-Cl distances in the coordination octahedron are 2.500 and 2.475 Å. The next-nearest-neighbor Mn ions are more than 4 Å away from these chlorines and it is unlikely that they contribute any significant portion of the transferred hyperfine interaction experienced by the chlorines. This situation is quite different from that in the anhydrous iron group halides. Even in the dihydrates  $\text{CuCl}_2 \cdot 2\text{H}_2\text{O}$ <sup>11</sup> and  $\text{CoCl}_2 \cdot 2\text{H}_2\text{O}$ ,<sup>12</sup> the chlorines are located at approximately equal distances from the magnetic ions.

The proton positions given by Zalkin, Forrester and Templeton are determined by the difference function method and are therefore considerably less accurate

than the positions of the other atoms. El Saffar and Brown<sup>13</sup> have recently re-examined the structure of  $\text{MnCl}_2 \cdot 4\text{H}_2\text{O}$  using neutron diffraction. The agreement in the proton positions given by the two methods is quite satisfactory but since the neutron-diffraction results appear to be more accurate they are used in this paper. Since both the x-ray work and neutron-diffraction work were done at room temperatures it is possible that the proton positions are slightly different at lower temperatures.

### III. EXPERIMENTAL

Temperatures in the range from the Néel temperature to 1.08°K were obtained with a conventional  $\text{He}^4$  system. Temperatures below 1°K were obtained using a simple glass  $\text{He}^3$  cryostat.<sup>14</sup> The  $\text{He}^3$  vapor pressure was measured with a NRC Alphanon and the values so obtained were converted to temperatures by calibrating the entire system against the susceptibility of potassium chrome alum.

In the antiferromagnetic phase both the proton and  $\text{Cl}^{35}$  lines were of sufficient intensity when detected with a simple marginal oscillator that they could easily be seen on the oscilloscope provided the temperature was

<sup>8</sup> B. R. Penfold and J. A. Grigor, *Acta Cryst.* **12**, 850 (1959).

<sup>9</sup> J. Mizuno, *J. Phys. Soc. Japan* **16**, 1572 (1961).

<sup>10</sup> J. Mizuno, *J. Phys. Soc. Japan* **15**, 1412 (1960).

<sup>11</sup> W. J. O'Sullivan, W. W. Simmons, and W. A. Robinson, *Phys. Rev.* **140**, A1759 (1965).

<sup>12</sup> A. Narath, *Phys. Rev.* **136**, A766 (1964).

<sup>13</sup> Z. M. El Saffar and G. M. Brown (private communication).

<sup>14</sup> J. A. Cowen, R. D. Spence, H. Van Till, and H. Weinstock, *Rev. Sci. Instr.* **35**, 914 (1964).

FIG. 2. Second-derivative recording of typical proton and chlorine lines in zero applied field. The line on the far left is a proton line. Those to the right are  $\text{Cl}^{35}$  lines with a small  $\text{Cl}^{37}$  line superimposed on the left-hand side of the left-hand line. Temperature:  $1.02^\circ\text{K}$ ; frequencies: proton, 9.81 Mc/sec;  $\text{Cl}^{35}$ , 9.38 and 9.16 Mc/sec.



$0.4^\circ\text{K}$  below the Néel temperature. To measure the width of these lines and to observe the weaker  $\text{Cl}^{37}$  lines, phase-sensitive detection was used to record the first derivative line shapes in applied field experiments and to record second derivative line shapes (see Fig. 2) in zero-field experiments. In the antiferromagnetic state the proton lines are  $\sim 45$  kc/sec wide and the chlorine lines  $\sim 15$  kc/sec wide. Below  $1^\circ\text{K}$  one observes a resolved dipole-dipole splitting of the proton lines which is approximately the same size as the high-temperature linewidth. Although the proton lines in the paramagnetic state are easily observed, repeated attempts to observe the chlorine lines in the *paramagnetic* state have all ended in failure. This is very unfortunate since a great deal of useful information about the chlorine system might be obtained if the lines could be detected in the paramagnetic state.

Zero-field experiments yield the magnitudes of the internal fields directly. The orientation of the internal fields can be determined either in an applied field or in zero field. In the latter method, the modulation field is supplied by a pair of Helmholtz coils which can be rotated about the axis of the helium Dewar. If the marginal oscillator is set at a frequency slightly above or below the value corresponding to the internal field, two lines appear on the oscilloscope which are centered on the point of zero modulation field on the time base, and which arise from two oppositely oriented internal fields of equal magnitudes. As the direction of the modulation field is changed the separation of the two lines changes and is at a minimum when the directions of the modulation field is as nearly parallel to the internal field direction as is possible for a given orientation of the crystal.

#### IV. PROTON RESONANCE

Table I summarizes the local fields found at proton sites at  $1.1^\circ\text{K}$ . The polar angle  $\vartheta$  is measured from the  $c_1$  axis and the  $\varphi$  is the azimuthal angle measured from the  $a_1^*$  axis in a plane perpendicular to  $c_1$ . There are eight distinct local field magnitudes, and except for the fields which lie in special orientations, there are four symmetry related orientations for each magnitude. The angular relation of the various local fields is shown in stereographic projection in Fig. 3. The stereogram follows the usual crystallographic convention that vectors in the upper hemisphere are indicated with solid circles while those in the lower hemisphere are indicated with open circles.

TABLE I. Local fields at proton sites at  $1.1^\circ\text{K}$ .

Field No.	$\vartheta$	$\varphi$	$H$ (oersteds)
1-2	0	0	5658
3-4	180	0	5658
5-6	42	$\pm 67$	3661
7-8	138	$\pm 113$	3661
9-10	35	$\pm 10$	3568
11-12	145	$\pm 170$	3568
13-14	38	$\pm 10$	3520
15-16	142	$\pm 170$	3520
17-18	75	$\pm 108$	2232
19-20	105	$\pm 72$	2232
21-22	78	$\pm 106$	1921
23-24	102	$\pm 74$	1921
25-26	78	$\pm 147$	1909
27-28	102	$\pm 33$	1909
29-30	65	$\pm 123$	1597
31-32	115	$\pm 57$	1597

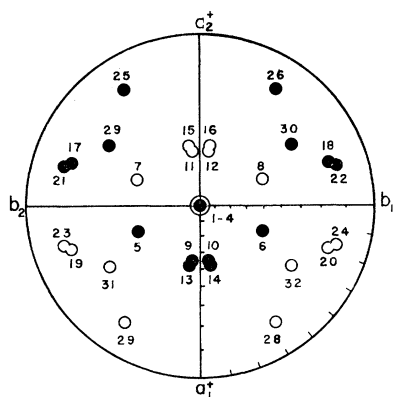


FIG. 3. Stereogram of the internal magnetic fields at proton sites. Axes are labeled for the alternate choices of unit cell.

The internal magnetic field<sup>15</sup>  $\mathbf{H}$  is a periodic function of the position vector  $\mathbf{r}$ . The elements of the Shubnikov group under which  $\mathbf{H}$  transforms are specified by giving two dyadics  $\Phi_i$  and  $\Theta_i$  and a translation  $\tau_i$  for each element such that

$$\mathbf{H}(\Phi_i \cdot \mathbf{r} + \tau_i) = \Theta_i \cdot \mathbf{H}(\mathbf{r}), \quad (1)$$

where  $\Phi_i$  acts on the components of  $\mathbf{r}$ ,  $\Theta_i$  acts on the components of  $\mathbf{H}$ , and the translation  $\tau_i$  is the vector sum of the translational component of the symmetry element and its displacement from the origin. The two dyadics are related by  $\Theta_i = \pm \Phi_i$  where the positive sign applies for ordinary elements which arise from rotation axes or for anti-elements which arise from rotatory inversion axes, and the negative sign applies for elements which arise from ordinary rotatory inversion axes or anti-elements which arise from rotation axes.<sup>16</sup>

The lack of a unique connection between  $\Theta_i$  and  $\Phi_i$  as indicated by the  $\pm$  sign shows that specifying the  $\Theta_i$  does not in general specify the *magnetic point group* of the crystal. A stereogram such as Fig. 3 implies a

TABLE II. Magnetic point groups having aspect  $2/m$ .

Magnetic point group	Number of elements	Number of distinct field magnitudes	
		$P$ cell	$P_c$ cell
$2'/m$	4	8	...
$2/m'$	4	8	...
$21'$	4	...	16
$m 1'$	4	...	16
$2/m 1'$	8	...	8

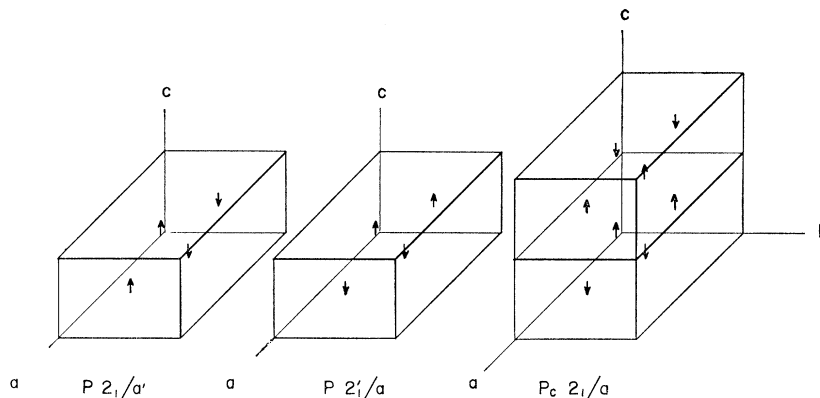
<sup>15</sup> Throughout this paper we have used the symbol  $\mathbf{H}$  for the internal magnetic field to conform with conventional usage. The symbol  $\mathbf{B}$  would be more appropriate since we deal here with the field inside a locally magnetized material. The latter choice is particularly desirable in dealing with the hyperfine interaction since if in the expression  $\mathbf{B} = 4\pi\mathbf{M} + \mathbf{H}$  one combines the "local" value of  $\mathbf{H} = -4\pi/3\mathbf{M}$  with  $4\pi\mathbf{M}$ , one immediately obtains the "contact" term  $8\pi/3\mathbf{M}$ . The Zeeman Hamiltonian  $\mathcal{H} = -\mathbf{u} \cdot \mathbf{B}$ , while unusual, is correct.

<sup>16</sup> J. D. H. Donnay and G. Donnay, *Compt. Rend.* 248, 3317 (1959).

definite set of  $\Theta_i$  which we shall call the *aspect* of the magnetic point group. The aspect of a magnetic point group may be designated by specifying the ordinary point group which would correspond to the set of  $\Theta_i$  if the vectors were polar vectors rather than axial vectors as they actually are. Thus there are 32 possible aspects for stereograms of the internal magnetic fields in crystals. In the present case the aspect is  $2/m$ . To each aspect there correspond several magnetic point groups which are obtained by considering the several possibilities implied by the  $\pm$  sign. Magnetic point groups containing the anti-identity  $1'$  (grey groups) can arise only from magnetic space groups which contain antitranslations. In the present case the permitted antitranslations and the magnetic unit cells which they generate are severely limited by the fact that two of the symmetry operations of the chemical space group, the screw axis and the glide planes, already have translational components of  $b_2/2$  and  $a_2/2$ , respectively. The introduction of antitranslations along these directions would modify the translational components of the screw and glide operations and locate field distributions corresponding to Mn ions at points where no Mn ions exist. Thus the only permitted antitranslation is along the  $c_2$  direction. The doubled magnetic unit cell generated by such an antitranslation we designate by  $P_c$ . Magnetic point groups which do not contain the anti-identity  $1'$  arise from magnetic space groups based on a magnetic unit cell identical with the chemical unit cell which in the present case is a primitive ( $P$ ) cell. In Table II we give the five magnetic point groups having aspect  $2/m$  and the number of elements in each group. The number of distinct local field magnitudes is equal to the number of protons in the *magnetic* unit cell divided by the number of elements in the magnetic point group. Since the observed number of local field magnitudes is 8 it is clear from Table II the only acceptable magnetic space groups are those having either magnetic point groups  $2'/m$  or  $2/m'$  and a  $P$  cell or the  $2/m 1'$  and the  $P_c$  cell. In each case the translation components to be added to the twofold axis and mirror plane to obtain the magnetic space groups must be the same as in the chemical space group if the singularities of the field are to coincide with the positions of the Mn ions. Thus the permitted space groups are  $P2_1/a'$ ,  $P2_1/a$  and  $P_c2_1/a$ . The spin arrangements corresponding to these groups are shown in Fig. 4.

To differentiate between the three groups one must compare the observed field magnitudes and directions with those calculated for each space group. If one assumes that the magnetic form factor of the Mn ions is spherically symmetric then the field at the proton sites is simply that of an array of point dipoles located at the Mn sites and whose direction is determined by the magnetic space group. The dipolar sum was computed for a sphere containing 5000 Mn ions surrounding a coordination octahedron. In the case of the groups

FIG. 4. Magnetic-moment arrangements consistent with the stereogram of Fig. 3 and the crystal structure of  $\text{MnCl}_2 \cdot 4\text{H}_2\text{O}$ . Axes correspond to the second set indicated in the text. Only the central figure— $P2_1/a$ —gives values of internal fields consistent with observations.



$P_c2_1/a$  and  $P2_1/a'$  the agreement between the observed and calculated fields was so poor that they could be discarded. In Table III we give a comparison between the observed field magnitudes and those calculated using the group  $P2'_1/a$  and indicate the angular difference in the orientation of the fields. In order to compare the field magnitudes we have assumed that the magnetic moment of the manganese ions is

$$\mathbf{u} = g\mu_B \mathbf{S}/r, \quad (2)$$

where  $g=2$ ,  $S=\frac{5}{2}$ ,  $\mu_B$  is the Bohr magneton and the quantity  $r=1.1845$  here represents the ratio of the proton internal fields at  $0^\circ\text{K}$  to those at  $1.1^\circ\text{K}$ . This ratio was obtained by extrapolating the proton frequency dependence to  $0^\circ\text{K}$ . In Fig. 5 we show the relation between the observed and calculated field magnitudes based on the magnetic moment given by Eq. (2). The fact that this value of magnetic moment also gives the good agreement between calculated and observed field magnitudes may be construed as indicating that there is negligible spin-wave reduction in the sublattice magnetization at  $0^\circ\text{K}$ . The discrepancies between the experimental and calculated field magnitudes shown in Fig. 5 are not understood. They are much larger than the error in the experimental fields. It is possible that the low-temperature proton positions differ significantly from the neutron-determined room-temperature positions. An alternate possibility would seem to be a small

interaction with the water oxygens which may in turn be subject to a small transferred hyperfine interaction with the manganese ions.

The temperature dependence of the zero-field proton and chlorine resonances is shown in Fig. 6. The proton data are shown as solid circles and the chlorine data as open circles. Measurement of all six of the  $\text{Cl}^{35}$  and three of the proton lines have been extended into the  $\text{He}^3$  temperature region. One proton line has been omitted from this diagram since it is essentially superimposed on the first line above the lowest frequency line. The data give no evidence for the phase transition at  $\sim 0.6^\circ\text{K}$  suggested by Abkowitz and Honig.<sup>17</sup>

## V. THE CHLORINE RESONANCE

In the absence of an applied field the Hamiltonian of the chlorine nuclei may be written

$$\mathcal{H} = -\gamma_n \hbar \mathbf{I} \cdot \mathbf{H} + \mathbf{Q} : \nabla \mathbf{E}, \quad (3)$$

where  $\mathbf{Q}$  and  $\nabla \mathbf{E}$  are the nuclear-quadrupole and field-gradient tensors and the internal field  $\mathbf{H}$  is given by

$$\mathbf{H} = \mathbf{H}_d - (\gamma_n \hbar)^{-1} \mathbf{A} \cdot \mathbf{S}. \quad (4)$$

Here  $\mathbf{H}_d$  is the dipolar field of the Mn ions,  $\mathbf{A}$  is the transferred hyperfine interaction tensor and  $\mathbf{S}$  is the

TABLE III. Comparison of observed fields with those calculated from  $P2'_1/a$ .

Experimental		Calculated $P2'_1/a$		
Field No.	Magnitude (oersteds)	Site (Fig. 1)	Magnitude (oersteds)	Orientation difference (degrees)
1-4	5658	4	5352	5
5-8	3661	2	3600	6
9-12	3568	1	3450	3
13-16	3520	3	3305	3
17-20	2232	8	2410	11
21-24	1921	5	1914	1
25-28	1909	7	2055	5
29-32	1597	6	1306	30

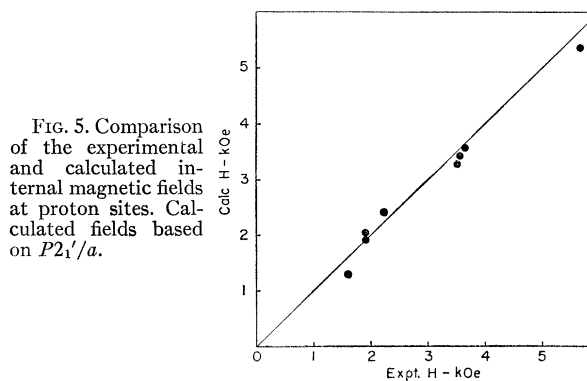


FIG. 5. Comparison of the experimental and calculated internal magnetic fields at proton sites. Calculated fields based on  $P2'_1/a$ .

<sup>17</sup> M. Abkowitz and A. Honig, Phys. Rev. 136, A1003 (1964).

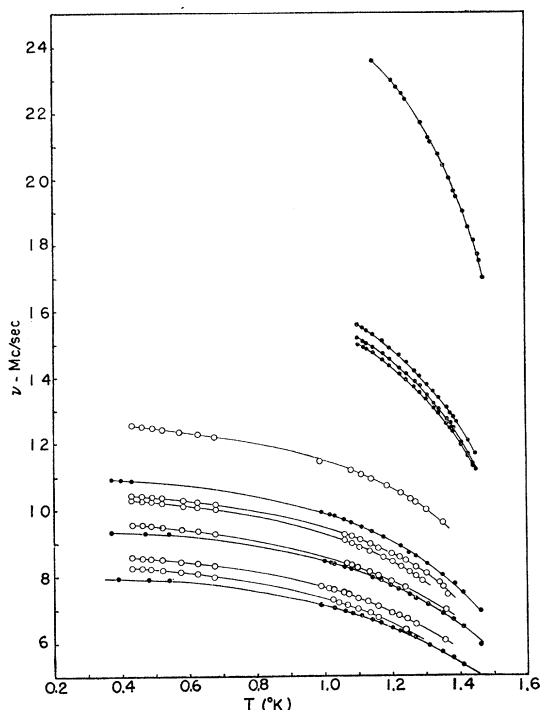


FIG. 6. Temperature dependence of the proton and chlorine lines in zero applied field. Solid circles—protons; open circles—chlorines. Only  $\text{Cl}^{35}$  lines are shown. One proton line which is essentially superimposed on the second proton line from the bottom has been omitted. The measurements on the upper set of proton lines were not extended below  $1^\circ\text{K}$  because of difficulties with the detectors when used with the  $\text{He}^3$  cryostat.

spin of the Mn ions. In view of our previous remarks concerning the crystal structure it appears that only the transfer hyperfine interaction between the Mn ions and the chlorine in the same coordination octahedron need be considered. Since the two chlorines belonging to a given octahedron are not related by symmetry operations, the tensors  $\mathbf{A}$  and  $\nabla\mathbf{E}$  are not necessarily equivalent for the two sites and may generate two distinct sets of lines. Furthermore the magnetic space group  $P2'_1/a$  which governs the transformation of the axial vectors, and the chemical space group  $P2_1/a$  which governs the transformation of the tensors leave the above Hamiltonian invariant at four symmetry-related sites in the cell. Thus the eight chlorines in the unit cell

TABLE IV. Zero-field chlorine resonance frequencies.

Set	$T = 1.06^\circ\text{K}$		$T = 0.43^\circ\text{K}$
	$\nu^{35}$ Mc/sec <sup>a</sup>	$\nu^{37}$ Mc/sec	$\nu^{35}$ Mc/sec
I 3	11.2546	9.2690	12.5258
I 2	9.0261	7.5045	10.3004
I 1	7.0876	5.9518	8.2537
II 3	9.2601	7.6579	10.4263
II 2	8.4051	...	9.5423
II 1	7.5173	6.3036	8.5753

<sup>a</sup> Probable error 5 kc/sec.  
<sup>b</sup> Obscured by proton line.

can lead to only two sets of lines. Since the temperature dependence of the frequencies of the chlorine lines is essentially the same as that of the protons it appears that the Zeeman term in the Hamiltonian dominates the quadrupole except perhaps in the immediate neighborhood of the Néel temperature. In such case only the three transitions which correspond to  $\Delta m = \pm 1$  are of appreciable intensity and should give three approximately equally spaced lines. Since the two chlorines are nonequivalent, one obtains two such sets of lines which are given in Table IV. The assignment of the various observed lines to one of the two sets was made on the basis of equal splitting and their behavior in a small applied field. The latter will be discussed in a subsequent paragraph.

The observed frequencies allow one to calculate the traces of the Hamiltonian directly. In terms of the three observed frequencies one finds for  $\Gamma_n = \text{trace}(\mathcal{H}^n)$

$$\Gamma_n = (\bar{\nu})^n + (\bar{\nu} + \nu_3)^n + (\bar{\nu} - \nu_2)^n + (\bar{\nu} - \nu_2 - \nu_1)^n, \quad (5)$$

where

$$\bar{\nu} = (\nu_1 + 2\nu_2 - \nu_3)/4. \quad (6)$$

TABLE V. Chlorine parameters at  $T = 1.06$  and  $0.43^\circ\text{K}$ .

Set	$\nu_0(1.06^\circ\text{K})$ (Mc/sec)	$\nu_0(0.43^\circ\text{K})$ (Mc/sec)	$\nu_Q[1 + \eta^2/3]^{1/2}$ (Mc/sec)
I	9.14	10.38	1.3
II	8.33	9.46	2.4

The second moment  $\Gamma_2$  is given by<sup>18</sup>

$$\Gamma_2 = 5\nu_0^2 + \nu_Q^2(1 + \eta^2/3), \quad (7)$$

where  $\nu_0 = (\gamma_n/2\pi)H$ ,  $\nu_Q = eQ(\partial E_z/\partial Z)/2h$ , and

$$\eta = (\partial E_x/\partial x - \partial E_y/\partial y)/(\partial E_z/\partial Z).$$

If  $\Gamma_2$  is determined at two temperatures  $T$  and  $T'$  such that  $T' < T$ , setting

$$r = H(T')/H(T), \quad (8)$$

one finds

$$\nu_0^2(T) = \{\Gamma_2(T') - \Gamma_2(T)\}/5(r^2 - 1), \quad (9)$$

and

$$\nu_Q^2[1 + \eta^2/3] = \{r^2\Gamma_2(T) - \Gamma_2(T')\}/(r^2 - 1), \quad (10)$$

where we have assumed that the pure quadrupole frequency  $\nu_Q$  and the asymmetry parameter  $\eta$  are temperature-independent in the temperature range  $T - T'$ . The temperature dependence of both the dipolar and hyperfine fields arises from the temperature dependence of the effective spin. Thus one may obtain the ratio  $r$  by measuring the ratio of internal fields at *proton* sites at temperatures  $T$  and  $T'$ . Typical results obtained by applying this method are given in Table V. Since the values of  $r$  obtained by this method are subject to considerable error the values of  $\nu_Q[1 + \eta^2/3]^{1/2}$  are not

<sup>18</sup> L. C. Brown and P. M. Parker, Phys. Rev. **100**, 1764 (1955).

very accurate. However they serve to justify the assumption that we deal with the high-field case. The errors in  $\nu_0$  are less serious because one does not lose significant figures quite as rapidly in the numerator of Eq. (9) as in Eq. (10).

The hyperfine field is obtained by subtracting the dipolar field from the total internal field. The orientation of the total internal field was determined by applying a small external field  $\delta\mathbf{H}$ . If  $\xi_{ik}$  is a unit vector in the direction of the  $i$ th ( $i=1, 2, 3, 4$ ) internal field of the  $k$ th set ( $k=I, II$ ) then from Eq. (7)

$$(\delta\nu_0)_{ik} = (\delta\Gamma_2)_{ik}/10(\nu_0)_k = (\gamma_n/2\pi)\xi_{ik} \cdot \delta\mathbf{H}. \quad (11)$$

To avoid the tedious computation of the shift in  $\Gamma_2$  at each angle it was found convenient to use the fact that in our case

$$\nu_0 \simeq (\nu_1 + \nu_3 + 2\nu_2)/4, \quad (12)$$

from which it follows that

$$(2\gamma_n/\pi)\xi_{ik} \cdot \delta\mathbf{H} \simeq (\delta\nu_1 + \delta\nu_3 + 2\delta\nu_2)_{ik}. \quad (13)$$

Figure 7 shows the angle dependence of the  $\delta\nu_3$ 's and  $\delta\nu_2$ 's for the two sets of lines obtained in a rotation about the  $a_1^*$  axis with  $\delta H = 250$  Oe. For the high-field case one obtains from perturbation theory the approximations

$$(\delta\nu_3)_{ik} = \delta\mathbf{H} \cdot \left[ \xi_{ik} \left( 1 + 3\frac{\nu_Q}{\nu_0}\alpha_k^2 + O\left(\frac{\nu_Q}{\nu_0}\right)^2 \right) + \zeta_{ik} \left( -3\frac{\nu_Q}{\nu_0}\alpha_k + O\left(\frac{\nu_Q}{\nu_0}\right)^2 \right) \right] (\gamma_n/2\pi), \quad (14)$$

$$(\delta\nu_2)_{ik} = \delta\mathbf{H} \cdot \left[ \xi_{ik} \left( 1 + O\left(\frac{\nu_Q}{\nu_0}\right)^2 \right) + \zeta_{ik} \left( O\left(\frac{\nu_Q}{\nu_0}\right)^2 \right) \right] (\gamma_n/2\pi), \quad (15)$$

$$(\delta\nu_1)_{ik} = \delta\mathbf{H} \cdot \left[ \xi_{ik} \left( 1 - 3\frac{\nu_Q}{\nu_0}\alpha_k^2 + O\left(\frac{\nu_Q}{\nu_0}\right)^2 \right) + \zeta_{ik} \left( 3\frac{\nu_Q}{\nu_0}\alpha_k + O\left(\frac{\nu_Q}{\nu_0}\right)^2 \right) \right] (\gamma_n/2\pi), \quad (16)$$

where  $\zeta_{ik}$  is a unit vector perpendicular to  $\xi_{ik}$  and lying in the plane of  $\xi_{ik}$  and the  $Z_k$  axis of the electric field gradient. Here  $\alpha_k$  is the cosine of the angle between the  $Z_k$  axis and  $\xi_{ik}$ . From Eqs. (14)–(16) it is clear that one expects quite different angle dependence for the shifts in the outer lines  $\delta\nu_3$ 's and  $\delta\nu_1$ 's as compared to the central lines  $\delta\nu_2$ 's. In fact the position of the maximum of  $\delta\nu_2$  gives a good approximation to the orientation of the internal field vector  $\xi_{ik}$ . From Fig. 7 it appears that both the vectors  $\xi_{iI}$  and  $\xi_{iII}$  lie very close to the  $a$ - $c$  plane. A corresponding rotation around the  $b$  axis

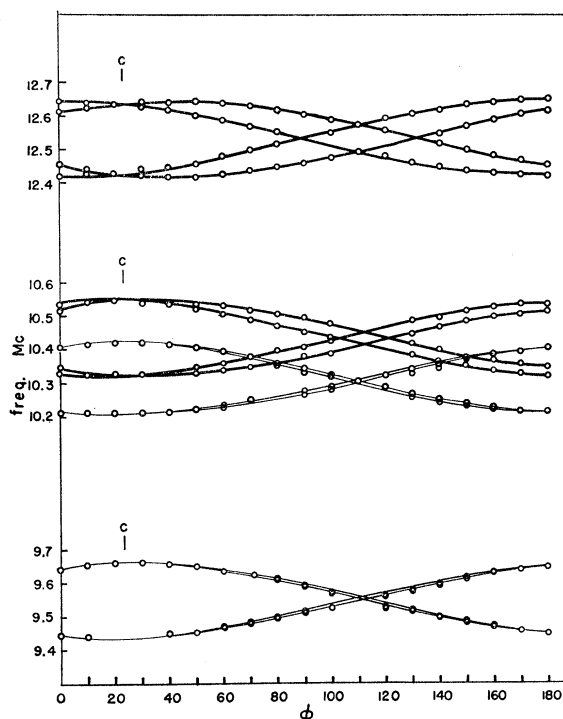


Fig. 7. Angle dependence of  $\delta\nu$  for  $\delta H = 250$  Oe. Rotation axis  $a_1^*$ ; temperature  $0.5^\circ\text{K}$ . Heavy curves: on top  $\delta\nu_3$  for set I; next set of heavy curves  $\delta\nu_3$  for set II. Light curves: middle  $\delta\nu_2$  for set I; bottom  $\delta\nu_2$  for set II.

shows that the internal field vectors  $\xi_{iI}$  are tilted  $13^\circ$  from the  $c$  axis towards  $a_1^*$  and the  $\xi_{iII}$  vectors are tilted  $1^\circ$  from  $c$  in the opposite direction.

We assume that the  $z$  principal axis of each of the two  $\mathbf{A}$  tensors lies along the corresponding Mn-Cl bonds. Since for Cl<sub>1</sub> the Mn-Cl<sub>1</sub> bond lies at  $66.5^\circ$  from the  $c$  axis, the  $c$  axis can not be a principal axis of its  $\mathbf{A}$  tensor. Since the spin direction is along  $c$ , any appreciable anisotropy in this tensor will result in a hyperfine field which lies considerably off the  $c$  axis. The calculated dipolar fields are quite small and therefore the *total* internal field should also lie considerably off the  $c$  axis. We therefore associate the experimental field of set I with Cl<sub>1</sub>, and as a consequence the internal field of set II with Cl<sub>2</sub>. The hyperfine field of Cl<sub>1</sub> calculated by subtracting the associated dipolar field from the experimental internal field lies in the plane of the Mn-Cl<sub>1</sub> bond, the  $c$  axis and the Mn-O<sub>1</sub> direction. Since the Mn-O<sub>1</sub> direction is  $90^\circ$  from the Mn-Cl<sub>1</sub> bond it must therefore constitute a second principal axis of  $\mathbf{A}^I$ . When the dipolar field is subtracted from the internal field for Cl<sub>2</sub> the hyperfine field lies exactly along the  $c$  axis. Thus for  $\mathbf{A}^{II}$  the  $c$  axis must be a principal axis. This is consistent with the fact that the Mn-Cl<sub>2</sub> bond lies at  $90^\circ$  from the  $c$  axis. Thus in the case of Cl<sub>1</sub> sites the spin is not along the axes and one obtains two of the elements of the hyperfine tensor while in the case of Cl<sub>2</sub> sites only one may be found. To calculate these

TABLE VI. Hyperfine-interaction elements for the two chlorine sites.

Element	Axis orientation	Value ( $\times 10^{-4}$ cm $^{-1}$ )
$A_{xx}^I$	Mn-O <sub>1</sub>	1.34
$A_{yy}^I$	$\perp$ to other two	...
$A_{zz}^I$	Mn-Cl <sub>1</sub>	1.08
$A_{xx}^{II}$	$\perp$ to other two	...
$A_{yy}^{II}$	$c$	1.16
$A_{zz}^{II}$	Mn-Cl <sub>2</sub>	...

elements one must estimate the value of the spin at 0°K. We have previously noted that the proton resonance gives  $S(0^\circ) \simeq \frac{5}{2}$  which is consistent with the specific-heat results of Miedema *et al.*<sup>19</sup> Values of the components of the hyperfine-interaction tensor are given in Table VI. The difference in the  $\mathbf{A}$  components for the Cl<sub>1</sub> sites may be taken as an indication of the  $p$ -orbital contribution. It is interesting to try to com-

<sup>19</sup> A. R. Miedema, R. F. Wielinga, and W. J. Huiskamp, *Physica* **31**, 835 (1965).

pare the order of magnitude of the components we obtain with those given by Shulman and Jaccarino<sup>20</sup> for MnF<sub>2</sub>. On reducing their value by the ratio

$$\frac{(\gamma_n)_{Cl} |\psi_{3s}(0)|^2_{Cl}}{(\gamma_n)_F |\psi_{2s}(0)|^2_F},$$

one obtains  $\mathbf{A} \sim 2.6 \times 10^{-4}$  cm $^{-1}$ . The agreement with our results is probably satisfactory since the Mn-cation distance is 2.11 Å in MnF<sub>2</sub> and 2.5 Å in MnCl<sub>2</sub>·4H<sub>2</sub>O.

#### ACKNOWLEDGMENTS

The authors take pleasure in acknowledging a number of very helpful suggestions from Dr. E. H. Carlson, Dr. J. A. Cowen, Dr. P. M. Parker, and Dr. H. Forstat. We should also like to thank R. Au for calculating the various dipolar sums and Jan Hessler for help in collecting the data. Special thanks are to be accorded Dr. Z. M. El Saffar for providing us with neutron-diffraction data on the proton positions.

<sup>20</sup> R. G. Shulman and V. Jaccarino, *Phys. Rev.* **108**, 1219 (1957).

## Nonvanishing Electric Field Gradients, Zero-Field Splitting, and Magnetic Field Energies of <sup>6</sup>S-State Ferric Ion in Tetragonal Symmetry

GILDA M. HARRIS\* AND MITCHELL WEISSBLUTH

*Biophysics Laboratory, Stanford University, Stanford, California*

(Received 17 February 1966)

A calculation has been made of the spin-orbit coupling of the high-spin ground state of ferric ion, the <sup>6</sup>S state, with excited doublet and quartet electronic states in strong crystal electric fields of tetragonal symmetry. The aim of the calculation was to simulate as closely as possible, without explicitly including bonding, the condition of ferric ion in the heme group of ferriheme compounds. Eigenfunctions and eigenvalues resulting from such a calculation were used as a basis for calculating other properties of interest of the ferric ion in such systems. Explicitly, the zero-magnetic-field splitting of the sextet ground state, magnetic-field energy components, effective magnetic moments, and the lattice and valence contributions to an electric-field gradient at the iron nucleus were calculated. These properties were investigated as a function of the cubic and tetragonal field strengths, the spin-orbit coupling strength, and the number of excited states included in the interaction. The calculated results were compared with existing experimental data from single-crystal electron spin resonance, magnetic-susceptibility measurements, and the observed quadrupole splitting of the Mössbauer resonance of high-spin ferriheme compounds. For a consistent and relatively narrow range of values for input parameters, all of the calculated properties agreed quite well with the experimental results currently available.

FERRIC ion in six-coordinated hemoglobin complexes with such ligands as H<sub>2</sub>O and F<sup>-</sup> in the sixth position, has a Mössbauer resonance (MR) spectrum which is split by the interaction of a nuclear quadrupole moment of the excited state of Fe<sup>57</sup> with a residual electric field gradient (EFG) at its nucleus.<sup>1</sup> Also, electron-spin-resonance (ESR) data indicate a

\* Present address: Department of Physics, Pomona College, Claremont, California.

<sup>1</sup> J. Maling and M. Weissbluth, in *Electronic Aspects of Biochemistry*, edited by B. Pullman (Academic Press Inc., New York, 1964).

nontrivial splitting of the <sup>6</sup>S ground state into three doubly degenerate components.<sup>2</sup>

These properties are not immediately apparent for an “S-state” ion. Such a ground state is not split by a crystal electric field. Nor is it split by first-order spin-orbit interaction of its six multiplet partners. Nor can the electron distribution of this 3d<sup>5</sup> spherically symmetric state, by itself, contribute to a nonzero EFG at the nucleus.

<sup>2</sup> D. J. E. Ingram, in *Paramagnetic Resonance*, edited by W. Low (Academic Press Inc., New York, 1963), Vol. II.